NASA CONTRACTOR REPORT   177441

Calculation of Helicopter Rotor Blade/Vortex Interaction
by Navier-Stokes Procedures

Y. -N. Kim
S. J. Shamroth
R. C. Buggeln

(NASA-CR-177441)   CALCULATION OF HELICOPTER   N88-13291
ROTOR BLADE/VORTEX INTERACTION BY
NAVIER-STOKES PROCEDURES Final Report
(Scientific Research Associates)   38 p   Unclas
Avail: NTIS HC A03/MF A01   CSCL 01A G3/02 0111704

NASA

Calculation of Helicopter Rotor Blade/Vortex Interaction
by Navier-Stokes Procedures

Y. -N. Kim
S. J. Shamroth
R. C. Buggeln
Scientific Research Associates
Glastonbury, Connecticut

NASA

National Aeronautics and
Space Administration

Ames Research Center
Moffett Field, California 94035

TABLE OF CONTENTS

ρ	Density
Γ	Strength of a vortex
$\vec{\Omega}$	Vorticity vector
C_p	Heat coefficient at constant pressure
d	$= \left\| \vec{r} - \vec{r}_c \right\|$; distance from a point on the centerline of a vortex
D	Jacobian of coordinate transformation
p, P	Pressure
r_0	Effective core radius
$\vec{r}$	Position vector
$\vec{r}_c$	Position vector of a point along the centerline
t	Time
T	Temperature
T_0	Stagnation temperature
$\vec{v}, \vec{V}$	Velocity vector
V_θ	Azimuthal velocity component
y	Distance from the solid wall
u, v, w	Cartesian velocity components in x, y and z direction
u', v', w'	Perturbed Cartesian velocity component due to an inserted vortex filament
U, V, W	Cartesian velocity components of background baseflow
(x, y, z)	Cartesian coordinates
$(\tilde{X}, \tilde{Y}, \tilde{Z})$	Coordinate system attached to some nominal center of a vortex
(ξ, η, ζ)	Computational coordinates

SUMMARY

Interactions of a modern rotor blade with concentrated tip vortices from the previous blades can have a significant influence on the airloads and the aeroacoustics of a helicopter. A better understanding of the blade/vortex interaction process and a method of analyzing its flow field would provide valuable help in the design of helicopters. The work discussed herein represents an initial effort in applying a three-dimensional, time-dependent Navier-Stokes simulation to the blade vortex interaction problem. The numerical technique is the Linearized Block Implicit (LBI) technique of Briley and McDonald. In this initial effort, consideration is given to the interaction of a wing of idealized geometry and a vortex whose axis is aligned at an arbitrary angle to the wing. The calculations are made for laminar, subsonic flow and show the time dependent pressure distribution and flow fields resulting from the interaction.

INTRODUCTION

Understanding and prediction of the flow field of a modern helicopter rotor blade is a problem of great practical importance. However, because of the inherent complexity of the flows surrounding a rotor blade, especially during forward flight, many important flow problems still require considerable further investigation (Johnson, 1986; McCrosky, 1986; Schmitz and Yu, 1986). One such problem is the unsteady transonic flow associated with a rotor blade interacting with concentrated tip vortices from the previous blades (Fig. 1). The interaction mechanism can have a significant influence on the airloads and the aeroacoustics of helicopter rotor blades. This is particularly true in the transonic flow regime, where shock-wave positions and strengths are sensitive to small changes in the flow parameters. The interaction between rotating blades and concentrated vortices is thought to be responsible for oscillatory blade loads, vibration and impulsive noise. Further, it has been conjectured that separation phenomenon may be taking place during a blade/vortex encounter of arbitrary orientation. The vortex field will induce a radial velocity component on the blade surface near the tip region (Fig. 2). This radial flow may occur in an adverse pressure gradient, possibly leading to separation. In addition, close encounters with a blade will probably alter the vortex core structure significantly and may lead to vortex bursting due to severe deformation.

A general procedure for predicting such a complicated flow field is a very demanding, yet very important task for investigation. Such a general prediction method would provide a major tool for both the research and the design engineer to improve both performance and aeroacoustics of a helicopter. Since the physical phenomena of these flows contain complex unsteady three-dimensional viscous and highly nonlinear effects, calculation techniques for predicting the detailed flow field must rely upon numerical approaches. This motivation has led to a major effort in developing numerical procedures of various degrees of sophistication. Some of the previous studies on transonic blade/vortex interaction analyses are briefly summarized here. Interaction between rotor blades and vortices can occur with various geometries, as shown in Fig. 3. These range from the hover case, where a trailing tip vortex is normal to a following blade, to forward flight, when the vortex and blades are nearly parallel under certain conditions. Most of the previous CFD analyses simplified the problem by
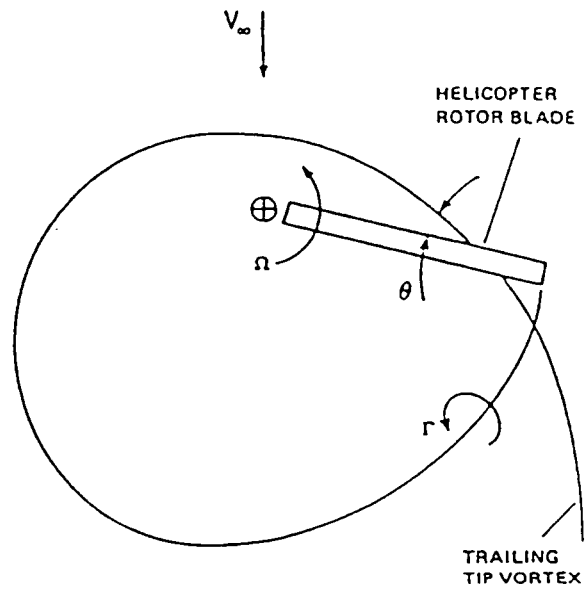
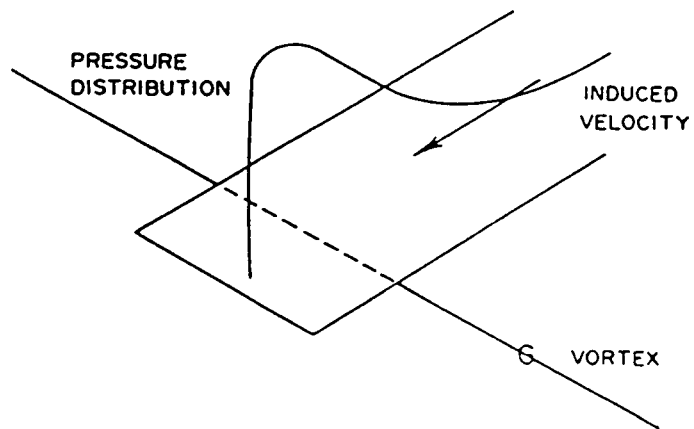Fig. 1 — Schematic of helicopter-rotor-blade/vortex interaction.

Fig. 2 — Schematic of flow field in the vicinity of tip due to blade/vortex interaction.

VORTEX NORMAL TO BLADE

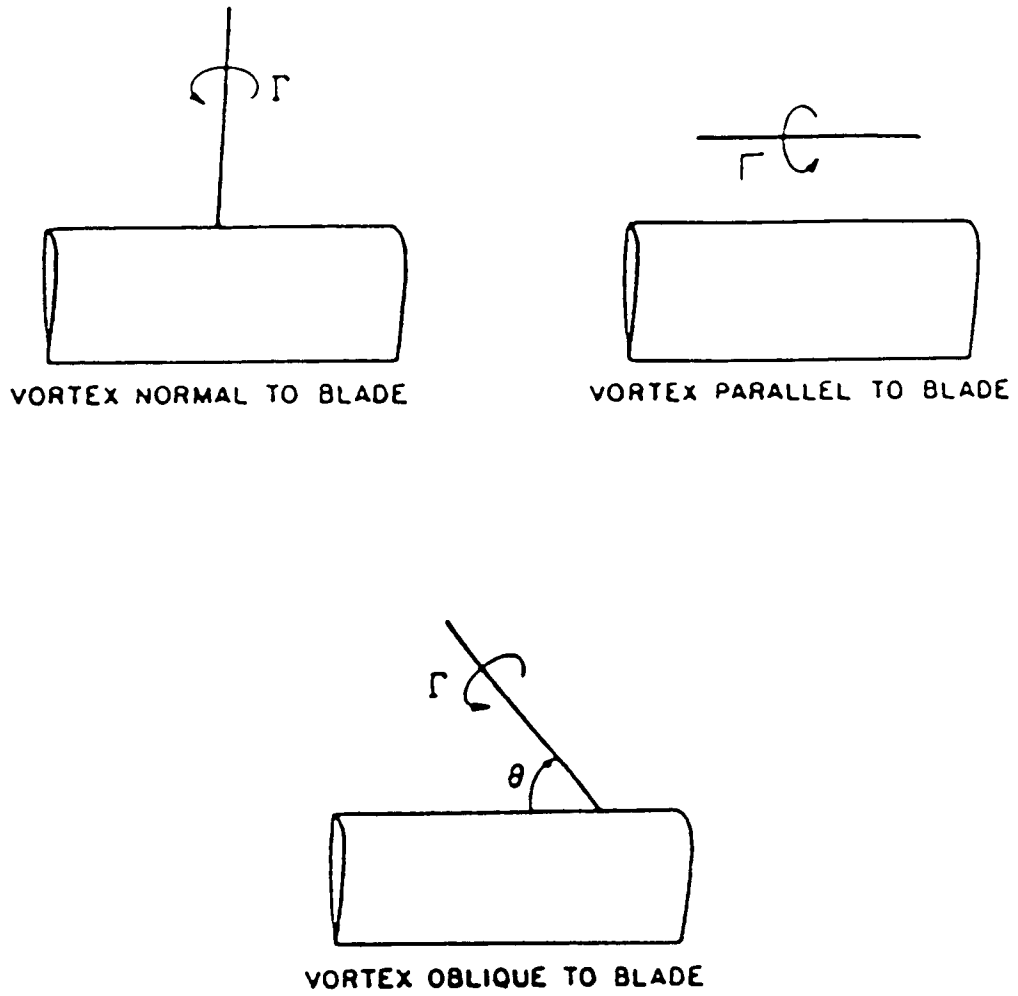VORTEX PARALLEL TO BLADE

VORTEX OBLIQUE TO BLADE

Fig. 3 - Types of blade/vortex interaction geometry.

limiting the encountering angle to zero or $\pi/2$; i.e., the vortex is either parallel or perpendicular to the blade. The interaction of the parallel vortex with the blade becomes a two-dimensional unsteady problem, while the perpendicular intersection of vortex with blade would be a three-dimensional steady problem. Some investigators, for example, George and Chang (1984) and McCroskey and Goorjian (1983), solved an unsteady two-dimensional small-disturbance potential equation to model the interaction of an airfoil with parallel vortex at transonic speed. Both Euler and Navier-Stokes equations (thin layer) were solved by other investigators (Srinivasan, McCroskey and Kutler, 1984; Hardin and Lamkin, 1984; Hsu and Wu, 1986; Rai, 1987) to simulate the same two-dimensional unsteady vortex interactions. On the other hand, either the small-disturbance potential equation or Euler equations were used to calculate the three-dimensional flow field when the vortex intersects with the blade at normal angle (Caradonna, Desopper and Tung, 1982; Srinivasan, Chyu and Steger, 1981). Since the helicopter rotor problem is very much three-dimensional and unsteady in nature, both two-dimensional unsteady and three-dimensional steady models are limited in their ability to provide information for the improvement of performance and aeroacoustic properties of a rotor blade. Moreover, the transonic small-disturbance calculation can cause errors in the important region near the leading edge unless special precautions are taken (McCroskey and Srinivasan, 1983). These considerations, combined with the potential viscous effects including shock-wave/boundary layer interactions, possible separation due to an adverse radial pressure gradient near the blade tip, and vortex instability leading to bursting due to severe deformation during close encounters, argue strongly for a Navier-Stokes approach to this problem. Furthermore, near-field of blade/vortex interaction (BVI) is strongly influenced by the leading edge boundary layer. For some types of BVI, generation of secondary vortices have been observed experimentally (Kaykayoglu and Rockwell, 1985). A Navier-Stokes approach, which also allows arbitrary vortex angle relative to the blade, is the focus of the present effort.

This effort represents an initial study in the application of the three-dimensional, time-dependent Navier-Stokes equations to the analysis of the transonic rotor blade/vortex interaction problem. It was designed to explore the basic features of blade/vortex interactions and to develop prediction methods for calculating such interactions in three dimensions under simplified geometry and flow conditions. The present effort focuses upon two tasks:

1) Generation of a grid system with special emphasis placed on the location of grid points to resolve the gradients of dependent flow variables within viscous regions. Then, as a baseline solution, obtain the steady state solution which could be used as initial conditions for the unsteady calculation.

2) Investigation of the modeling method of an incident free vortex and then, based upon the chosen model, calculate the time-dependent flow around the blade interacting with an oncoming vortex to demonstrate the capability of the present Navier-Stokes approach. Finally, analyze the results to assess the capability of the proposed numerical procedure and the effects of a vortex on the unsteady airloads.

ANALYSIS

General Considerations

As a first step in applying the three-dimensional, unsteady Navier-Stokes equations to the transonic rotor blade/vortex interaction (BVI) effects on an

actual helicopter performance and noise, the problem of a vortex interacting
with a blade section was investigated for a simple blade geometry. The
techniques to be investigated and demonstrated apply equally to more complex
geometric configurations, including rotor blade tips. However, in the present
effort, the emphasis is on a demonstration of the basic aerodynamic phemnomena,
and this does not require the more complex geometries.

The innovation of the present study is twofold. First is the inclusion of
the viscous effects in the computations, thus allowing the vortex structure to
change as the flow proceeds downstream, allowing blade viscous displacement
effects to influence the vortex path, etc. Secondly, in the present study, a
vortex is allowed to encounter a blade at an arbitrary angle, unlike the
previous studies which were limited to either 0° or 90°.

Governing Equations

The unsteady, three-dimensional, compressible Navier-Stokes equations,
supplemented by an equation of state and together with the constant total
temperature assumption, form the system governing the flows in the present
effort. The total temperature assumption was made solely to conserve computer
run time and can be easily removed through inclusion of an energy equation.
The specific scalar momentum equations to be solved are the x, y and z Cartesian
momentum equations. The dependent variables chosen are the physical Cartesian
velocities u, v, w and the density, ρ.

The equations are then transformed to a computational coordinate system in
which the computational coordinates (ξ, η, ζ) are related to the Cartesian
coordinates (x, y, z) by

$$\xi = \xi(x,y,z,t)$$
$$\eta = \eta(x,y,z,t)$$
$$\zeta = \zeta(x,y,z,t) \qquad (1)$$
$$\tau = t$$

Use of the general coordinate system allows solid boundaries to be specified as
coordinate lines. This, in turn, allows accurate application of boundary
conditions at wall no-slip surfaces, which has proven to be a very important
consideration in obtaining an efficient and accurate solution procedure. Since,
in general, the computational coordinates may be a function of time with a
time-dependent Jacobian, the equations are cast into the so-called 'strong
conservation form' (Thomas and Lombard, 1979):

$$\frac{\partial W/D}{\partial \tau} + \frac{\partial}{\partial \xi} \left(\frac{W\xi_t}{D} + \frac{F\xi_x}{D} + \frac{G\xi_y}{D} + \frac{H\xi_z}{D} \right) + \frac{\partial}{\partial \eta} \left(\frac{W\eta_t}{D} + \frac{F\eta_x}{D} + \frac{G\eta_y}{D} + \frac{H\eta_z}{D} \right)$$

$$+ \frac{\partial}{\partial \zeta} \left(\frac{W\zeta_t}{D} + \frac{F\zeta_x}{D} + \frac{G\zeta_y}{D} + \frac{H\zeta_y}{D} \right) = \frac{\partial}{\partial \xi} \left(\frac{F_1\xi_x}{D} + \frac{G_1\xi_y}{D} + \frac{H_1\xi_z}{D} \right) \qquad (2)$$

$$+ \frac{\partial}{\partial \eta} \left(\frac{F_1\eta_x}{D} + \frac{G_1\eta_y}{D} + \frac{H_1\eta_z}{D} \right) + \frac{\partial}{\partial \zeta} \left(\frac{F_1\zeta_x}{D} + \frac{G_1\zeta_y}{D} + \frac{H_1\zeta_z}{D} \right)$$

and

$$p = \rho RT \tag{3}$$

$$T_0 = T + \frac{q^2}{2C_p} = \text{constant} \tag{4}$$

where

$$D = \begin{vmatrix} \xi_x & \xi_y & \xi_z \\ \eta_x & \eta_y & \eta_z \\ \zeta_x & \zeta_y & \zeta_z \end{vmatrix} \tag{5}$$

and

$$W = \begin{bmatrix} \rho \\ \rho u \\ \rho v \\ \rho w \end{bmatrix}, \quad F = \begin{bmatrix} \rho u \\ \rho u^2 + p \\ \rho u v \\ \rho u w \end{bmatrix}, \quad G = \begin{bmatrix} \rho v \\ \rho u v \\ \rho v^2 + p \\ \rho v w \end{bmatrix}$$

$$H = \begin{bmatrix} \rho w \\ \rho u w \\ \rho v w \\ \rho w^2 + p \end{bmatrix}, \quad F_1 = \begin{bmatrix} 0 \\ \tau_{xx} \\ \tau_{xy} \\ \tau_{xz} \end{bmatrix}, \quad G_1 = \begin{bmatrix} 0 \\ \tau_{xy} \\ \tau_{yy} \\ \tau_{yz} \end{bmatrix}, \quad H_1 = \begin{bmatrix} 0 \\ \tau_{xz} \\ \tau_{yz} \\ \tau_{zz} \end{bmatrix} \tag{6}$$

Equation (2), as supplemented by Eqs. (3)-(6), forms the governing equations for the system.

Model of the Incident Free Vortex

Although the present study determines the dynamic interactions of a vortex with a blade via a solution of time-dependent, three-dimensional Navier-Stokes equations, it is necessary to specify an initial flow field, i.e., a flow field at $t = 0$, which includes an initial vortex structure. The initial vortex is approximated by a slender tube-like region of infinite length in which the bulk of vorticity is concentrated, as in Fig. 4. Tip vortex generation is excluded from the present study. Over each cross-section of this tube-like region, a mean direction, $\vec{e}_s$, as well as the strength, Γ, of the concentrated vorticity can be determined. Further, inside of this compact region, a spatial curve can be found such that its tangent is parallel to $\vec{e}_s$ at each cross-section. This spatial curve is considered as the effective centerline of the slender yet highly vortical region. The position vector of this effective centerline is denoted by $\vec{r}_c$ and a segment of this line is denoted by $d\vec{s} = ds \vec{e}_s$.
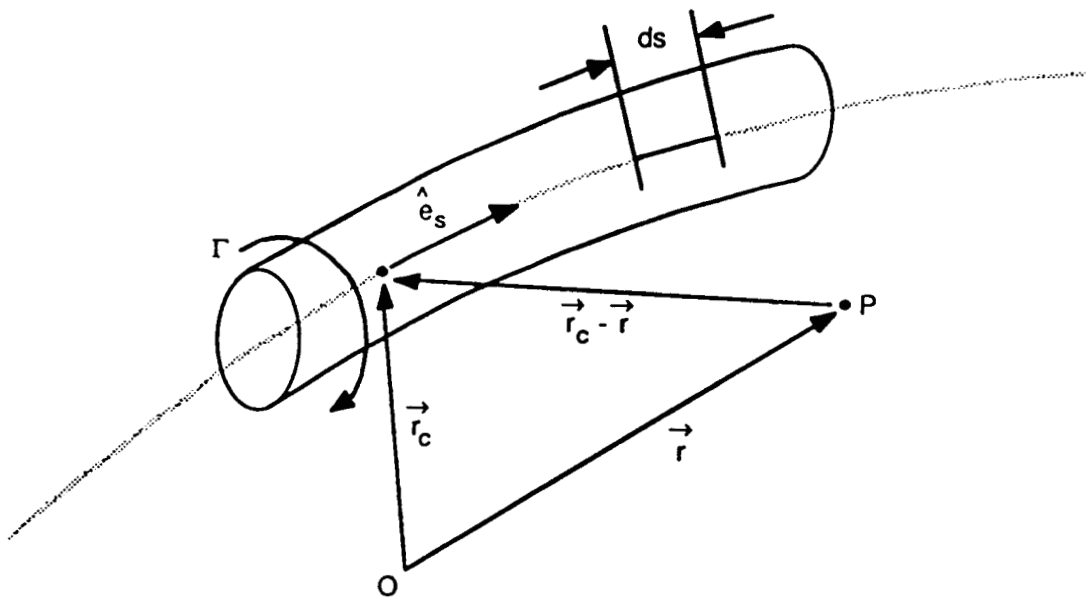
-6-

Fig. 4 – A schematic of a vortex

When viewed from a region sufficiently far from the effective centerline, the slender vortex is reduced to a curved line vortex of strength, Γ, and with position vector, $\vec{r}_c$. The signature of the vortex in this outer region is then the induced velocity field given by the Biot-Savart law:

$$\vec{v}(\vec{r}) = -\frac{1}{4\pi} \int_c \frac{\Gamma \cdot (\vec{r}_c - \vec{r})}{\left| \vec{r}_c - \vec{r} \right|^3} \times d\vec{s} \tag{7}$$

where $\vec{r}$ is the position vector of a point, P, in the space and $\vec{r}_c$ is the position vector of a point along the line vortex, C.

However, when a point, P, is located in the proximity of the vortex, the effects of the inner structure of the vortex on the induced field must be taken into account. Although this can be accomplished by using a so-called optimum similarity solution (Ting, 1980) to prescribe the diffusive core structure, the present work employs a simpler model to account for the influence of the diffusive vortex core by multiplying the induced velocity obtained in Eq. (7) with a factor (Liu, Shamroth and McDonald, 1986).

$$f(d, r_0) = \frac{d^2}{d^2 + r_0^2} \tag{8}$$

where $d = \left| \vec{r} - \vec{r}_c \right|$ and r_0 is the effective core radius. Note that if the solid-body-rotation model were used for simulating the core structure, the multiplying factor would be the minimum between 1 and d^2/r_0. A model of the tip vortex as a whole must induce a shear layer within the pre-existing boundary layer around a blade section such that the induced velocity field also satisfies the no-slip condition on the wall. Very little is known about the structure of this induced, unsteady shear layer. The present model of the tip vortex neglects the detailed structure of an induced shear layer in the vicinity of the wall. It is assumed that the effect of their presence is to provide a rapid change of the induced velocity field in the region very close to the wall such that the no-slip condition is satisfied. These effects are accounted for by multiplying the induced velocity fields with a factor (Liu, Shamroth and McDonald, 1986).

$$g(y) = \ell(y)/\ell_0 \tag{9}$$

where y is the distance from the wall and

$$\ell(y)/\ell_0 = \tanh(ky/\ell_0) \mathcal{D} \tag{10}$$

with

$$\mathcal{D} = 1 - \exp(-y/\ell_1) \tag{11}$$

and k is the von Karman constant; ℓ_0 and ℓ_1 are some characteristic length scales. In the present work, both ℓ_0 and ℓ_1 are assumed to be equal to an estimated boundary layer thickness. Since this model of induced shear layer is used only for constructing the initial induced flow field associated with an inserted vortex, and not used in the subsequent calculations, rough estimation of characteristic length scales does not affect the final results.

As mentioned before, the tip vortex is generally curved during its interaction with a blade. The Biot-Savart integral, i.e. Eq. (7), for a curved

vortex filament formally contains singular terms. Although these singular terms can be removed by analytical cancellation (Ting, 1980) in addition to the prescription of models of diffusive core structure such as the one given by Eq. (8), considerable mathematical and computational complexities are involved with the evaluation of the induced velocity field of a curved vortex filament. The present work assumes that the precise shape of the tip vortex is not of major importance; therefore, for simplicity in setting the initial flow field for the Navier-Stokes simulation, the tip vortex will be assumed to be straight. However, it should be emphasized that this assumption is not required during unsteady simulation of blade/vortex interactions, i.e., the vortex filament is allowed to deform during its convection downstream. For a straight vortex filament, the Biot-Savart law reduces to a simple form as

$$V_\theta = \frac{\Gamma}{2\pi d} \tag{12}$$

Thus, the signature or the induced velocity field of the tip vortex modeled by a straight line vortex filament at a point, p, with position vector, $\vec{r}$, is then given by

$$\vec{V}(\vec{r}) = f(d, r_0) \times \frac{\Gamma}{2\pi d} \times g(y)$$

with

$$f(d, r_0) = \frac{d^2}{d^2 + r_0^2} \tag{13}$$

and

$$g(y) = \tanh(k_y / \ell_0)\left[1 - \exp(-y/\ell)\right]$$

where c is the effective centerline of the vortices and $d = \left|\vec{r}_c - \vec{r}\right|$. The corresponding vorticity distribution is obtained from

$$\vec{\Omega} = \nabla \times \vec{V} \tag{14}$$

In the present study, an interaction of a vortex with a blade at an arbitrary orientation is the major focus. For the unsteady computation, a vortex filament could be placed in the baseline background flow at swept angle to generate the initial induced flow field. Estimation of the induced flows can affect the initial start-up of the computation. However, an alternate procedure to induce an orientation of the vortex filament was utilized. The fundamental concept of this procedure is to put a straight vortex filament in a flow field which varies linearly in the axial direction of the vortex as shown in Fig. 5. Initially, the vortex filament is oriented in the spanwise direction of the blade. However, as the vortex convects at local flow velocity, the vortex gradually changes its orientation and interacts with a blade at non-zero intersection angle. As a result of this procedure, estimation of the initial flow field becomes straightforward. In addition, it should be noted that in the actual rotor case an observer sitting on the rotor does see an oncoming flow with a spanwise gradient.
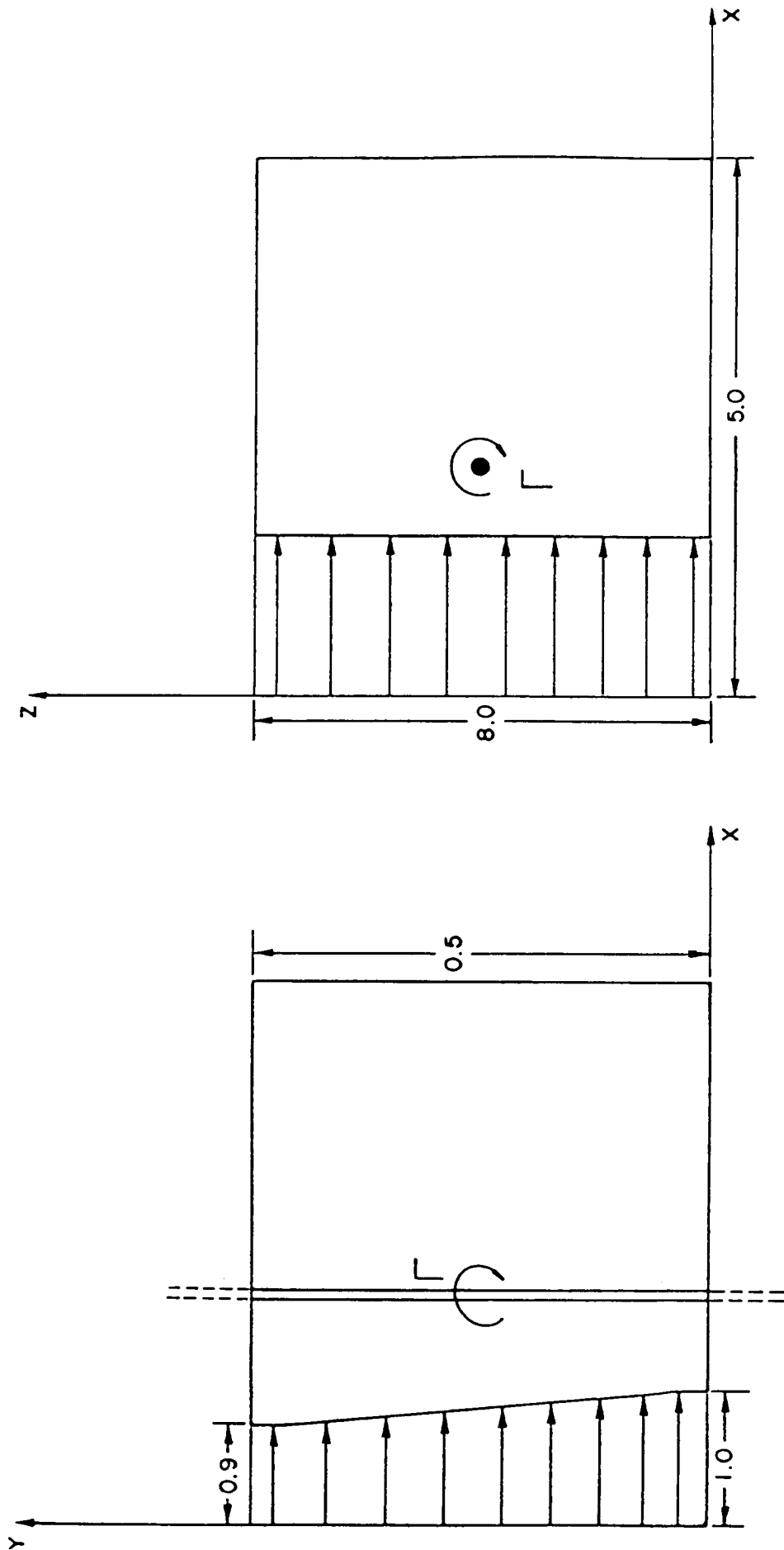
Fig. 5 - A schematic of the three-dimensional computation of a vortex in a sheared flow

At any instant, the composite flow is considered as consisting of the background flow and the variation from the background flow. Obviously, such a variation contains not only the evolution of the initially introduced tip vortex, but also the subsequent distortion of the background flow due to this vortex. Let (u,v,w,p) denote the Cartesian velocity components and the pressure of the composite flow observed in a ground-fixed system (x,y,z) where x is in the streamwise direction, y is the distance normal to the wall and z is in the spanwise direction, then

$$u(x,y,z,t) = u'(x,y,z,t) + U(x,y,z) \qquad (15)$$

$$v(x,y,z,t) = v'(x,y,z,t) + V(x,y,z) \qquad (16)$$

$$w(x,y,z,t) = w'(x,y,z,t) + W(x,y,z) \qquad (17)$$

$$p(x,y,z,t) = p'(x,y,z,t) + P(x,y,z) \qquad (18)$$

where U, V, W and P are the velocity components and the pressure of the background flow which is considered as nominally steady. The variations from the background flow are denoted by (u',v',w',p').

Solutions of the governing equations with specified Reynolds number and freestream Mach number subjected to prescribed initial conditions, and appropriate boundary conditions are sought by a numerical solution procedure. Generally speaking, the initial condition, as well as the boundary conditions, depend on the initial arrangement of the introduced vortex. The current effort focuses upon the dynamical effects of a straight line vortex filament, submerged and convected in a baseline steady flow around the blade, modeled as a flat semi-infinite plate with thickness.

The base background flow is supplied by performing the usual Navier-Stokes calculation, as will be discussed in detail subsequently. The initial, induced velocity field associated with the introduced straight line vortex filament is constructed with the aid of Biot-Savart law, supplemented by modifications accounting for the effects of a diffusive vortical core and the effects of an induced internal shear layer, as described by Eq. (13). Since the induced velocity is obtained with Biot-Savart integral, this field is evaluated with respect to a coordinate system $(\tilde{x},\tilde{y},\tilde{z})$ which is attached to some nominal center of the vortex. Note that this center can be in motion. It is assumed here that, at t = 0, a fixed vortex is suddenly introduced into some region of the background flow such that

$$u'(x, y, z, t = 0) = \tilde{u}(\tilde{x}, \tilde{y}, \tilde{z},)$$

$$v'(x, y, z, t = 0) = \tilde{v}(\tilde{x}, \tilde{y}, \tilde{z},)$$

$$w'(x, y, z, t = 0) = \tilde{w}(\tilde{x}, \tilde{y}, \tilde{z},)$$

with

$$x = \tilde{x} + X_0$$

$$y = \tilde{y}$$

$$z = \tilde{z} + z_0$$

i.e., this initially fixed nominal vortex center is located at the midpoint of the vortex span, and it has a streamwise position, $x = x_0$. As mentioned before, $\tilde{u}$, $\tilde{v}$ and $\tilde{w}$ are obtained from Eq. (13).

Thus the incipient conditions for u, v and w are completely prescribed. The incipient condition for the composite pressure field, p, must be specified in such a way that it is consistent with the prescribed composite velocity field. By noting that (i) the induced field falls off rapidly in regions away from the vortex, and (ii) over a very short time span, $\Delta t \rightarrow 0$; it is quite valid to consider the induced field as frozen. Then, the starting pressure field of the composite flow can be obtained by using the prescribed velocity field and by solving the Poisson equation of pressure subjected to the following boundary conditions (Liu, Shamroth and McDonald, 1985).

$$p(\tilde{r} \rightarrow \infty, t = 0) = P(\tilde{r} \rightarrow \infty) \tag{19}$$

i.e., $p' \rightarrow 0$ as $\tilde{r} \rightarrow \infty$. It should be noted that this condition is used only to compute starting pressure field consistent with the frozen induced flow field obtained from the Biot-Savart law. The effects of this condition on the final far-field unsteady pressure field is assumed negligible.

In the present effort, the pressure field induced (by an embedded vortex) is determined by introducing a further physical assumption. For simplicity, the vortex is assumed to be located in a uniform steady base flow. Then, the pressure can be obtained by integrating the radial momentum equation

$$\frac{dp}{dr} = \frac{\rho V_\theta^2}{r}$$

where r is the radius and V_θ is the velocity component in the circumferential direction.

A consistent, incipient density field of the composite flow must also be supplied. In general, this can be accomplished by several iterations between the results of the integration of the radial momentum equation and the solution of the equation of state. For nearly incompressible or low Mach number flow cases, such an iteration procedure usually can be by-passed.

As for the boundary conditions, no-slip condition is applied on the wall plane and the density on this plane is calculated from the normal momentum equation. The streamwise boundary conditions used in the present simulation specify upstream velocity profiles and downstream static pressure distributions. The three-dimensional case allows for spanwise variation of the streamwise component of velocity on the upstream boundary. Other velocity components were set equal to zero. However, for the two-dimensional case upstream total pressure was specified instead of the streamwise velocity component. The upstream total pressure determines the actual values of the streamwise velocity

component at the inflow section. Other velocity components and the second derivative of the static pressure are set to be zero. At the downstream boundary, the pressure is specified and the second derivative of all velocity components are set to be zero. On a plane (or a line for a two-dimensional case) which is parallel to the rigid wall, and is located sufficiently away from the outer edge of the boundary layer, the pressure distribution is specified and the second derivatives of all velocity components are considered as zero. These boundary conditions are expected to be appropriate so long as the inflow, outflow and the outer freestream planes are sufficiently far away from the evolving vortex throughout the course of the simulation. For the three-dimensional case, in view of the present approach to the modeling of the blade/vortex interactions, symmetrical conditions are applied as boundary conditions on the plane in the spanwise direction (Fig. 6).

Numerical Procedure

The numerical procedure used is a consistently split, linearized block-implicit (LBI) scheme described by Briley and McDonald (1977; 1980). The method can be briefly described as follows: the governing equations are replaced by an implicit time difference approximation. Terms involving nonlinearities at the implicit time level are linearized by Taylor series expansion in time about the solution at the known time level, and spatial difference approximations are introduced. The result is a system of multidimensional, coupled (but linear) difference equations which is solved in block-implicit form using an ADI scheme with consistent intermediate steps. For a linear scalar diffusion equation, this algorithm reduces to a classical ADI scheme considered by Douglas and Gunn (1984). Warming and Beam (1977, 1978) have introduced a very concise derivation of this algorithm using approximate factorization of the linearized approximation written in 'delta' form. Further development and applications have been investigated by Pulliam and Steger (1980), Thomas and Lombard (1979) and Shamroth, McDonald and Briley (1984) and others.

The method centers around the use of a formal linearization technique adapted for the integration of initial-value problems. The linearization technique, which requires an implicit solution procedure, permits the solution of coupled nonlinear equations in one space dimension (to the requisite degree of accuracy) by a one-step noniterative scheme. Since no iteration is required to compute the solution for a single time step, and since only moderate effort is required for solution of the implicit difference equations, the method is computationally efficient; this efficiency is retained for multidimensional problems by using ADI techniques. The method is also economical in terms of computer storage, in its present form requiring only two time-levels of storage for each dependent variable. Furthermore, the ADI technique reduces multidimensional problems to sequences of calculations which are one-dimensional in the sense that easily-solved narrow block-banded matrices associated with one-dimensional rows of grid points are produced. Consequently, only these one-dimensional problems require rapid access storage at any given stage of the solution procedure, and the remaining flow variables can be saved on auxiliary storage devices if desired. Since each one-dimensional split of the matrix produces a consistent approximation to the original system of partial differential equations, the scheme is termed a consistently split linearized block implicit scheme. Consistent splitting has been shown by a number of authors (e.g. Briley and McDonald, 1980) to considerably simplify the application of the intermediate split boundary conditions.
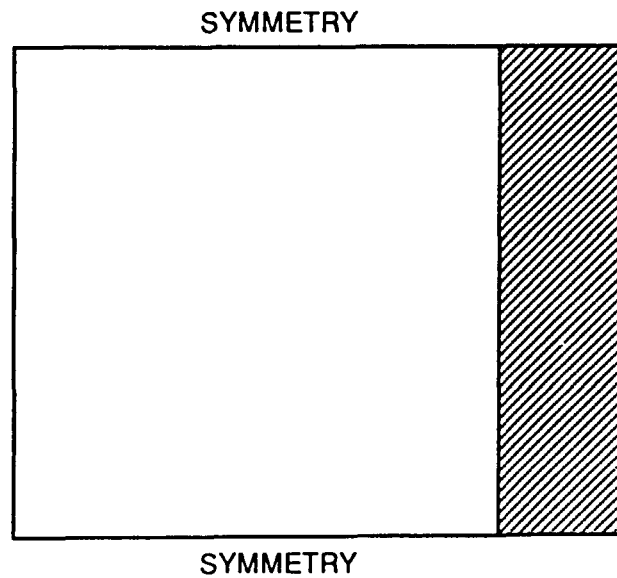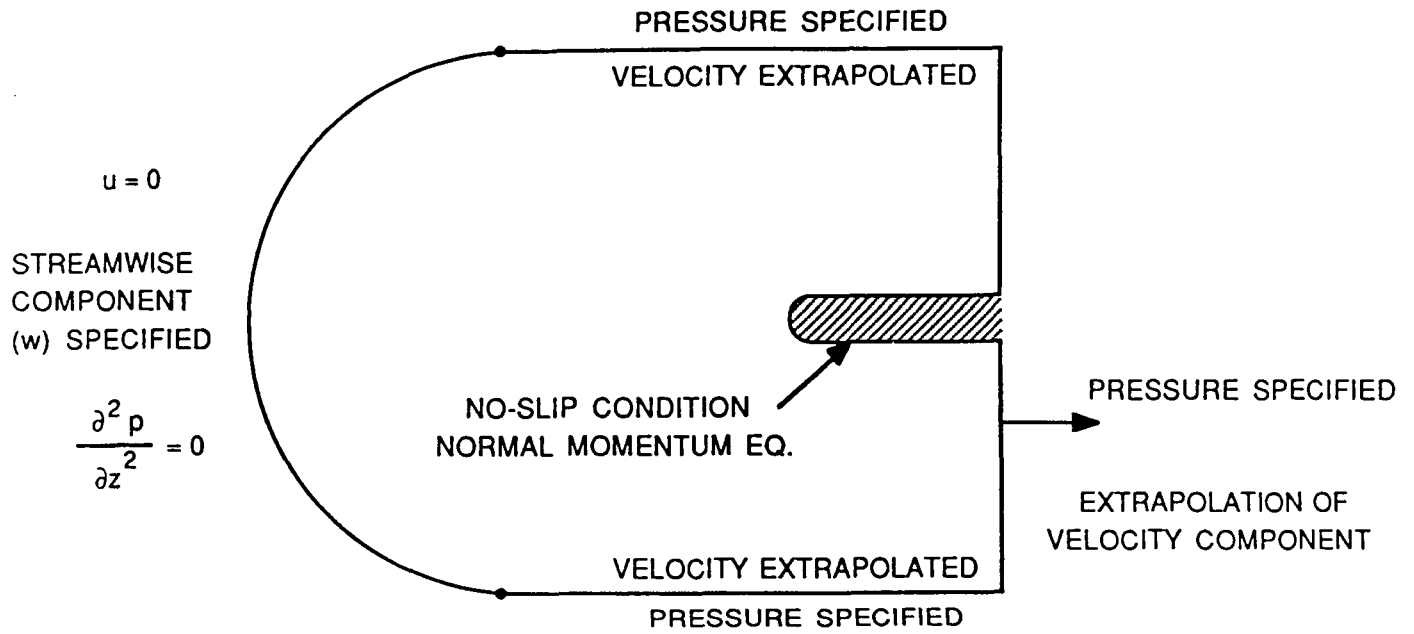
PRESSURE SPECIFIED

VELOCITY EXTRAPOLATED

u = 0

STREAMWISE
COMPONENT
(w) SPECIFIED

$$\frac{\partial^2 p}{\partial z^2} = 0$$

NO-SLIP CONDITION
NORMAL MOMENTUM EQ.

PRESSURE SPECIFIED

EXTRAPOLATION OF
VELOCITY COMPONENT

VELOCITY EXTRAPOLATED

PRESSURE SPECIFIED

SYMMETRY

SYMMETRY

Fig. 6 – Boundary conditions for three-dimensional case.

-14-

Under the current effort, the major goals were (1) to generate a grid system and perform a steady base flow calculation, and (2) to investigate a modeling method of an incident free vortex and to perform a time-dependent flow simulation based upon the chosen vortex model. Then the results are analyzed to assess the feasibility of the method utilized in the present study. As a means to achieve these goals more effectively, subtasks were added. These are (1) to investigate a two-dimensional case for the qualitative comparison with other existing computational results, and (2) to assess the numerical stability of the computation when a vortex convects in a sheared flow without a blade.

As discussed previously, the present effort focused upon the investigation of the unsteady three-dimensional flow associated with the interactions of the blade with vortices for a relatively simplified geometry and flow conditions. This configuration assumes an elliptical leading edge geometry which does not vary with span (Fig. 7). Similarly, the computational region is limited to the leading edge interaction region, thus computing the flow in the region upstream of the airfoil and the portion of the blade, as shown in Fig. 8. The computation domain is that enclosed within boundary ABCDEFGA of Fig. 8. Further, the flow is currently assumed to be subsonic and laminar. This allows the present effort to focus upon demonstrating the basic interaction fluid dynamic phenomena via a Navier-Stokes simulation without including the more complex geometric and flow condition effects at this time. Basic strategy of the present study is shown in a simplified flow chart in Fig. 9.

The Coordinate System

The choice and construction of a coordinate system is an important component in the successful solution of the blade/vortex interaction problem based upon the Navier-Stokes approach. Therefore, generation of a viable system is mandatory. The coordinate system must resolve flow regions such as boundary layers and vortex where rapid flow field change occurs. Finally, coordinates should allow accurate implementation of boundary conditions. The specification of boundary surfaces which do not fall upon coordinate lines or at specific grid points may present a difficult problem for Navier-Stokes analyses. Thus, a body-fitted coordinate system is generated in the present work.

Many alternative approaches are available for generating body-fitted coordinates, although in general they can be categorized into three generic groups. These are conformal, algebraic and elliptic. In the present work, the constructive algebraic approach has been adopted. The grid system obtained through the constructive approach requires a calculation or specification of arc lengths on the boundaries. Then, the distribution of grid points on and within the boundaries are obtained based on the parameterized length. A grid distribution is required which obtains high grid resolution in regions where rapid flow variations are expected. In particular, a cluster of grid points is required in the regions of both the free vortex and the boundary layer. This is accomplished by the use of a hyperbolic tangent function. A typical C-grid generated by this method is shown in Fig. 10. The grids of Fig. 10 are 113 × 50 in size (but 99 × 35 for the two-dimensional case) and extend four chord lengths in the radial direction. The spacing of the first node normal to the surface is 1.3×10^{-2} chords. The present grid distribution was assessed against a more tightly packed grid distribution in the boundary layer region. Comparison
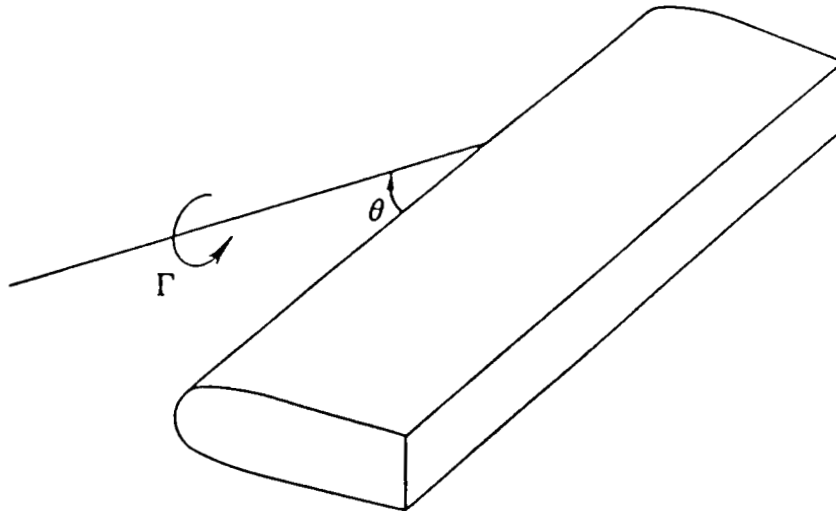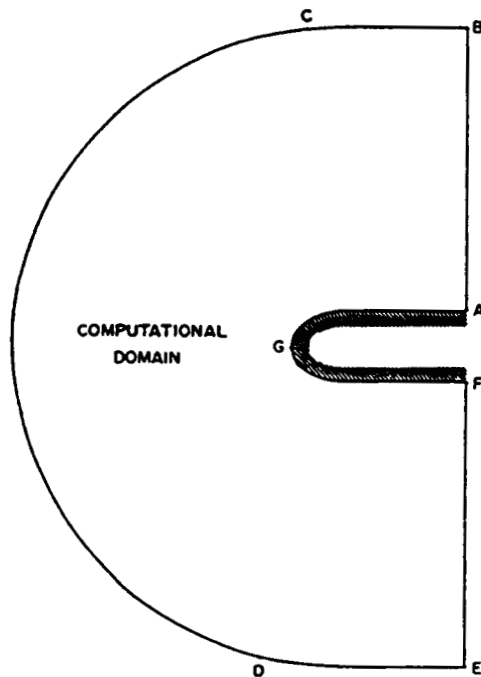
Fig. 7 - Flow geometry

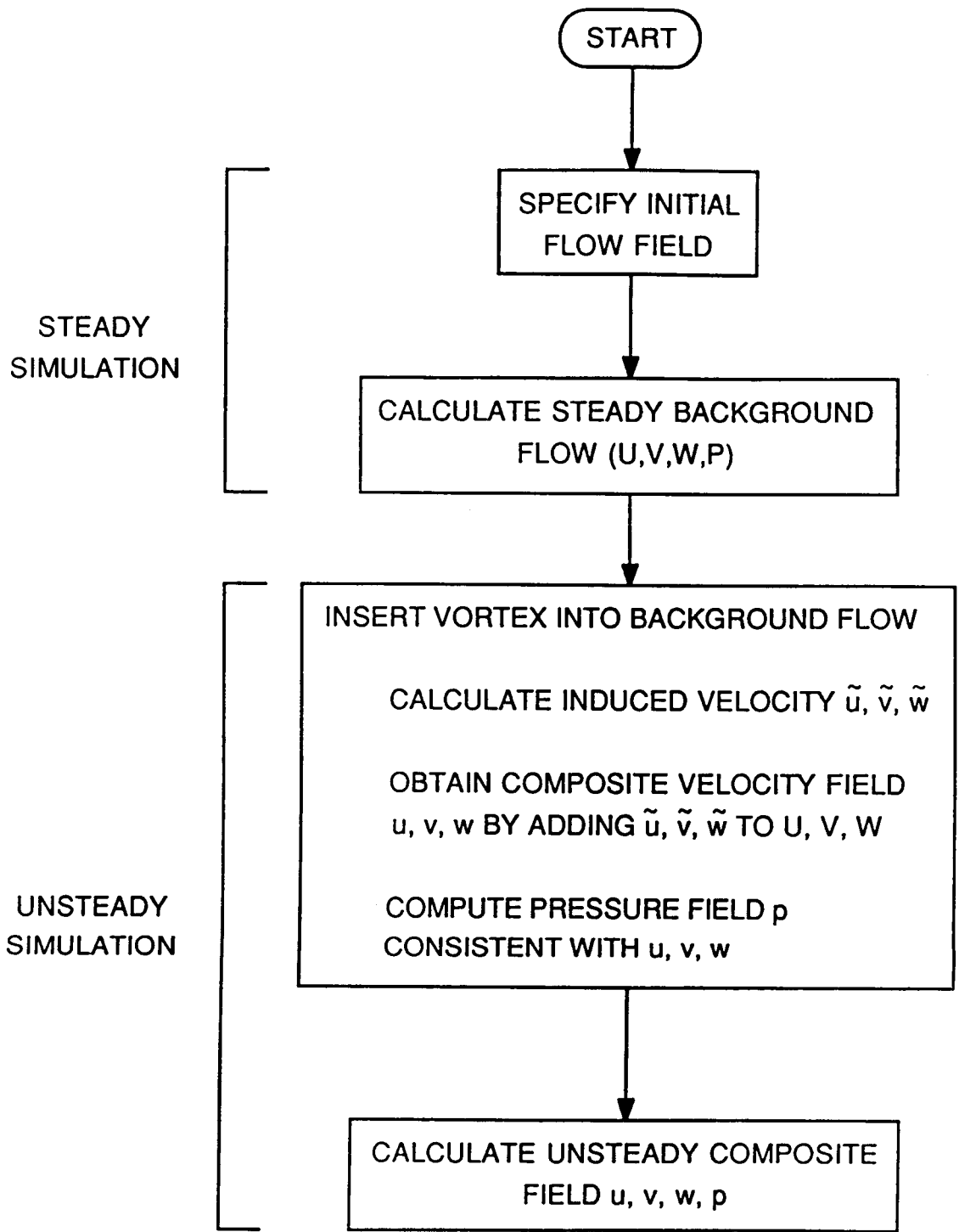Fig. 8 - A schematic of computational domain (side view)

START

STEADY
SIMULATION

SPECIFY INITIAL
FLOW FIELD

CALCULATE STEADY BACKGROUND
FLOW (U,V,W,P)

UNSTEADY
SIMULATION

INSERT VORTEX INTO BACKGROUND FLOW

CALCULATE INDUCED VELOCITY $\tilde{u}$, $\tilde{v}$, $\tilde{w}$

OBTAIN COMPOSITE VELOCITY FIELD
u, v, w BY ADDING $\tilde{u}$, $\tilde{v}$, $\tilde{w}$ TO U, V, W

COMPUTE PRESSURE FIELD p
CONSISTENT WITH u, v, w

CALCULATE UNSTEADY COMPOSITE
FIELD u, v, w, p
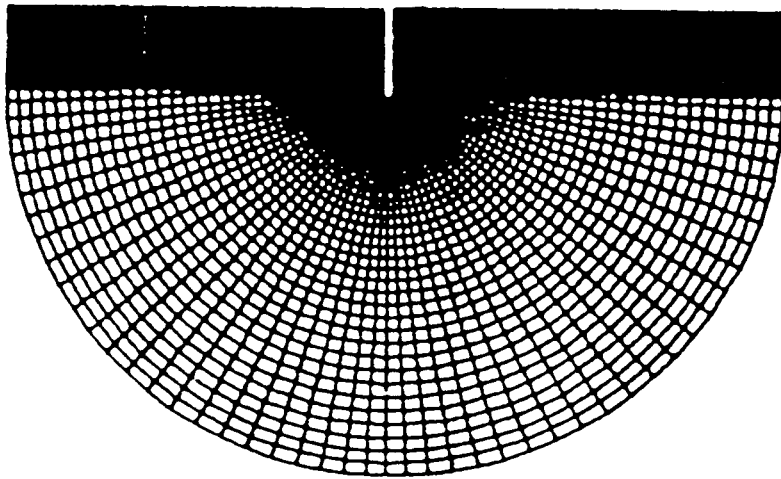
Fig. 9 — A flow chart of computational strategy

Fig. 10 – Computational grids (side view)

indicated that coarse grid distribution in the boundary layer does not affect the pressure distribution. Thus, more grid points could be distributed to maximize the resolution along the path of a vortex. For a three-dimensional case, the domain extends one chord length in the spanwise direction. Thirty spanwise mesh points were distributed uniformly. Preliminary investigation using a vortex filament in the sheared flow, as described later, indicated no need to use a non-uniform distribution.

Two-Dimensional Results

Having generated a viable coordinate system, the next step in the process is to obtain a solution of the Navier-Stokes equations for the specified coordinate system and flow conditions. Before computing the proposed three-dimensional case, a limiting case for a zero vortex interaction angle is considered as a means to get useful experience and information for the three-dimensional case to be considered later (Fig. 11). Since this has been a popular case among many investigators, it is expected that a qualitative validation against the other existing calculations can be obtained even if geometry and flow conditions are somewhat different.

The analysis consists of two steps. First, a steady base flow is obtained by converging the solution of Navier-Stokes equations. Then, a vortex of the specified size and strength is inserted into the steady base flow by adding the induced flow field consistent with the governing equations. This composite flow field is used as initial conditions for the unsteady simulation of blade/vortex simulation. The computation was performed at subsonic Mach number under laminar flow conditions. The Mach number was 0.4 and the Reynolds number was 200, based on the blade chord length. Mesh points used in this two-dimensional calculation are 99 and 35 points in the circumferential and radial direction respectively. As shown in Fig. 10, the computation utilized a C-type grid system. Baseline flow field is represented by the steady state solution of a stationary blade section in a uniform freestream. The blade section considered is a thin semi-infinite blade with an elliptical leading edge shape. The flow moves at zero angle of attack. In this case, it is not necessary to accurately follow the transient motion, and indeed it may be advantageous, from a computational efficiency viewpoint, not to follow the transient motion accurately if this accelerates convergence to the steady state. The present approach utilizes the matrix conditioning technique of Briley, McDonald and Shamroth (1983) to accelerate convergence to a steady state. The steady state solution so obtained for a blade section is shown by the symbol Δ in Fig. 12 in terms of coefficients of pressure (C_p).

Insertion of a vortex into the steady baseline flow destroys the symmetry of a C_p distribution around the blade where t indicates the ellapsed time after the vortex is inserted. The vortex was initially positioned at a location upstream of the blade (x_0, z_0) and then made to convect with the flow. The strength of the vortex initially located at ($x_0 = 2.5$, $z_0 = -0.25$) was $\Gamma = 1.0$. In order to obtain the composite flow field to be used as initial conditions for the time-dependent simulation, the vortex-induced flow field was computed as described previously. The vortex was assumed to have a core size of radius equal to 0.1.

Computational results for the case considered are presented in the form of C_p plots and both vortex contours in Figs. 12 and 13 at several temporal
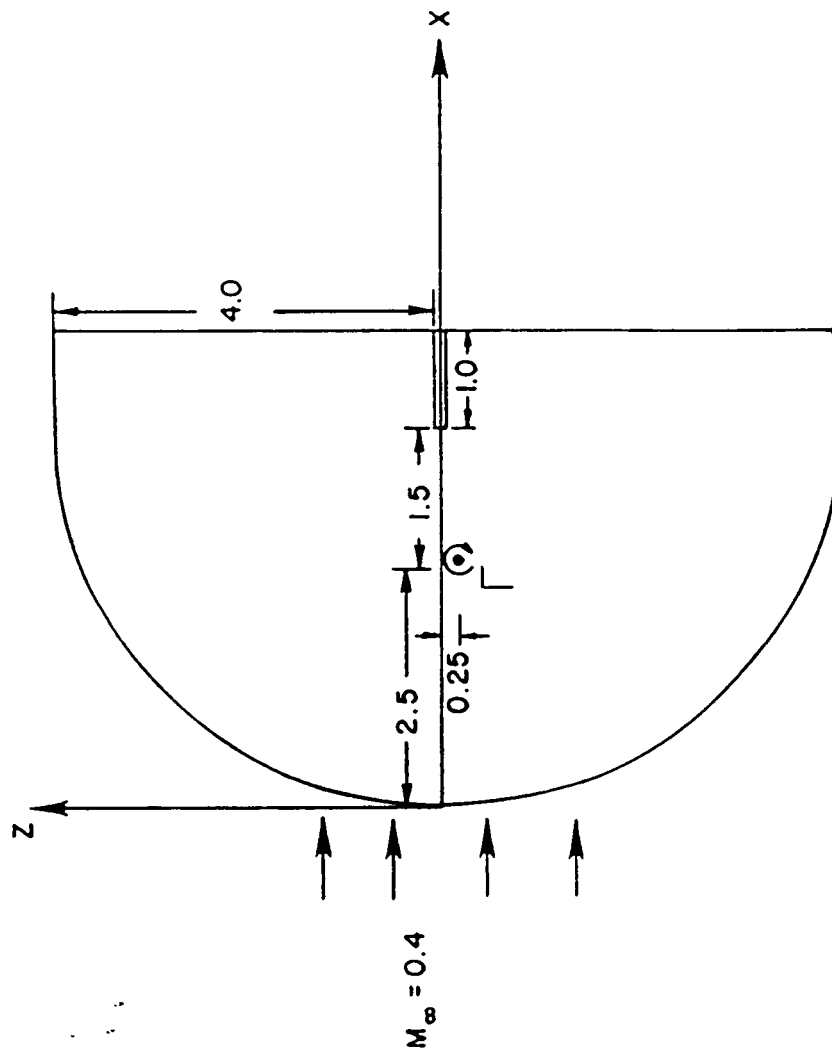
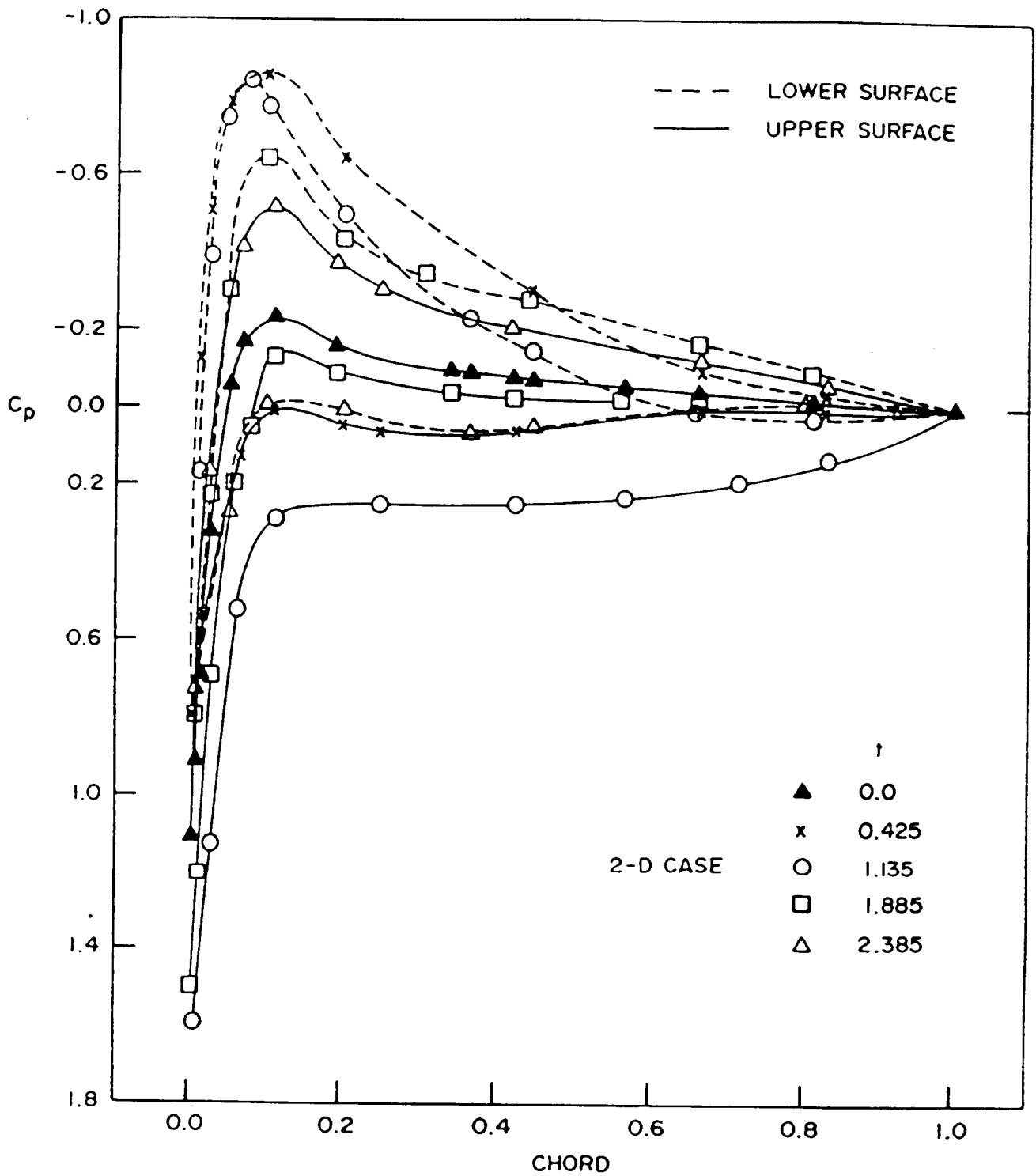Fig. 11 – A schematic of two-dimensional computation of blade/vortex interactions

Fig. 12 – Unsteady surface pressure distribution
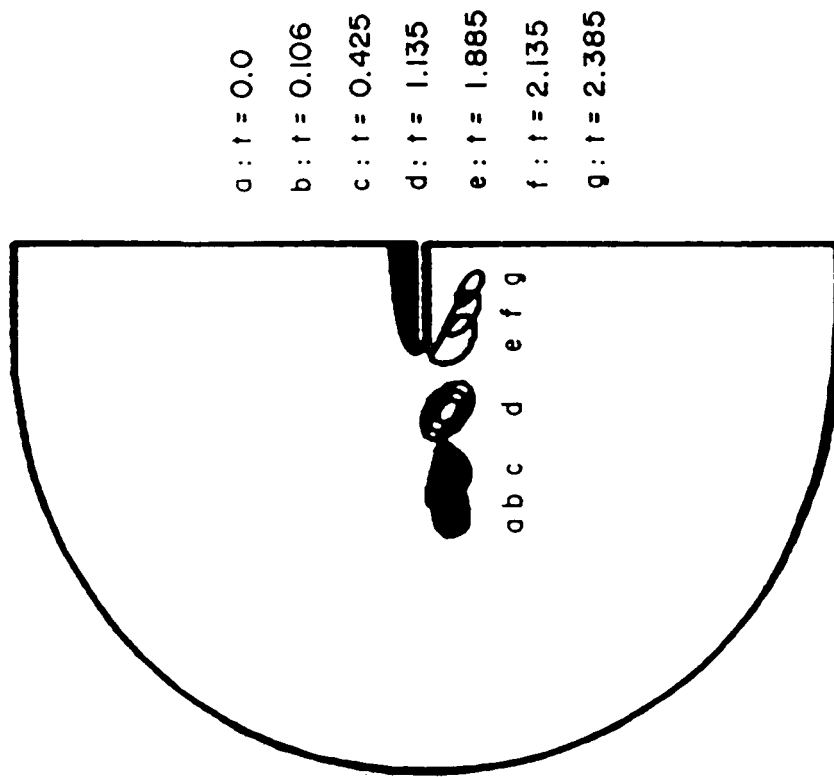(two-dimensional case)

a : t = 0.0
b : t = 0.106
c : t = 0.425
d : t = 1.135
e : t = 1.885
f : t = 2.135
g : t = 2.385

Fig. 13 – Vorticity contours during vortex/blade interaction (two dimensions)

stages (ellapsed time) of vortex movement. The pressure distribution, (C_p), presented in Fig. 12, generally illustrates the evolution of the BVI effects. Figure 13 shows the computed solution in terms of vorticity contours during the vortex/blade interaction. The figure shows a sequence of plots illustrating the evolution of a vortex which was inserted upstream. The vortex was located one and one-half chord lengths upstream and 0.25 below the chord line. For this calculation, the initial radius of the vortex was 0.1 and its strength, defined in terms of circulation, was 1.0. As shown in the figure, the vortex is deformed and diffused rapidly as it approaches the blade. The size and strength of the vortex was chosen such that it can reach the leading edge of the blade with strength enough to induce observable unsteady flow field at this low Reynolds number. It should be noted that to identify the convecting vortex effectively, only positive vorticity contours in the range of 0.0 to 8.0 were plotted at intervals of 0.5.

It is observed that the vortex decelerates as it begins to feel the presence of a blade section. The trajectory is also deflected due to the mean flow field around the blade. The vortex, which was originally circular, is distorted in shape due to the velocity gradient associated with the blade mean flow. Such distortion leads to a substantial increase in the diffusion of the vortex, particularly at this low Reynolds number condition. As a result, the vortex after the interaction becomes very weak, as shown. The effects of mesh distribution must still be investigated. Figure 12 shows the evolution of static pressure distribution while a vortex passes underneath the blade. At t = 0, steady pressure distrubution shows that there is no lift generated due to the symmetry of the configuration. However, when a vortex is inserted and allowed to convect with the moving stream, the flow field becomes asymmetric as a result of negative angle of attack (downward effect). As a result, negative lift force is generated, as inferred from the figures. The trend of lift force vector agrees qualitatively with other works (Srinivasan, McCroskey and Kutler, 1984; Hardin and Lamkin, 1984; Hsu and Wu, 1986), i.e., an inserted positive vortex induces negative lift force which increases in magnitude as the vortex approaches the blade section. As soon as the vortex core passes the leading edge, the trend reverses.

Three-Dimensional Results

The primary objective of the present study is to compute the BVI when the interaction occurs at arbitrary intersection angle. The analysis requires a specification of the induced flow field for the time-dependent simulation. One way to let the vortex convect at swept angle is to construct the induced flow field of the swept, but straight, vortex filament of a finite core size and combine it with the uniform flow. The procedure to generate a consistent initial induced flow field based upon this approach is feasible, but complex. In the present study, an alternative method was utilized to generate a swept vortex convecting with steady base flow. The base flow is assumed to be sheared in the spanwise direction so that the straight vortex filament in the flow can be allowed to change its orientation slowly as it is convected downstream. This sheared baseline flow models a rotor blade of a helicopter which has mean flow linearly varying in the radial direction. However, a question arose as to the stability of the vortex column in the spanwise direction under the influence of a sheared mean flow. Therefore, it was decided to perform a computational experiment under the idealized flow situation. The blade was excluded from the consideration to simplify the problem. The simulation was performed in the

physical domain, as illustrated in Fig. 5. A grid of 50 × 22 × 35 points were distributed in x, y and z direction, respectively. When the steady state solution was obtained, a vortex of the same size and strength as used in the two-dimensional case was introduced into the background flow through the induced flow field. The background flow varies linearly from 0.9 to 1.0 in the spanwise direction. A straight vortex filament inserted in the baseline flow is estimated to have an intersection angle of approximatly 10°. Computational results, as shown in Fig. 14, confirmed that the vortex is stable in the spanwise direction. The figure shows the contours of the velocity component in z-direction on the plane which passes through the vortex center. These contours, primarly due to the induced field of the vortex, clearly illustrate the orientation of the vortex.

After the successful confirmation that the vortex does not develop instabilities in the spanwise direction, a final three-dimensional case was considered (Fig. 15). The computational domain utilized in this case is obtained by extending the two-dimensional domain in the spanwise direction. The same Mach and Reynolds numbers as for the two-dimensional case were used in the computation. Based upon the experience of both two- and three-dimensional preliminary cases, vortex magnitude and core size were changed to 1.5 and 0.2. To obtain the best resolution of the flow field, 113 × 50 × 30 mesh points were distributed in the circumferential, radial and spanwise direction, respectively. The mesh points were uniformly distributed in the spanwise direction. In order to produce a little larger intersection angle at the encounter of the vortex with blade, the spanwise variation of the freestream was changed. It should be noted that this is imposed at the upstream boundary as a boundary condition. In the present three-dimensional case, the velocity component varies from 0.8 to 1.0. When a blade is present in the flow, the vortex convects at slower speed, in particular in the neighborhood of the leading edge. The actual intersection angle should be expected to be smaller than that estimated based upon the freestream flows. The initial vortex-induced flow field was assumed not to change in the spanwise direction. However, as the vortex changes its orientation, as well as experiences the axial stretching, the spanwise velocity gradually develops. The computational results are presented in Figs. 16-18. The results are shown at two different spanwise locations, i.e. 0.138 and 0.828, to illustrate the effects of BVI due to the swept vortex filament. Fig. 16 presents the contours of the vorticity component in the direction perpendicular to the paper. The ranges of the contours were limited from 0.0 to 8.0 at intervals of 0.5 in order to identify the moving vortex filament. The figure clearly indicates that the vortex encounters the blade section earlier, at y = 0.828. The intersection angle estimated from the figure is approximately 13 degrees. The contour plots indicate that the vorticity magnitude at the center of core reduces by a factor of 3 before reaching the leading edge. As discussed in the two-dimensional case, physical diffusion at this low Reynolds number is believed to contribute to the substantial diffusion of the vortex, however, mesh studies are still required. Figures 17 and 18 show the plots of the blade surface pressure distribution as a function of time at two spanwise locations. As expected from experience with the two-dimensional case, the vortex initially induces downwash effects (negative angle of attack) on the blade. Negative lift force results from the negative angle of attack. As the vortex core approaches the leading edge, the magnitude of lift force increases. The trend changes the other way after the vortex passes the leading edge. The vortex induces upwash effects and thus reduces the lift force.
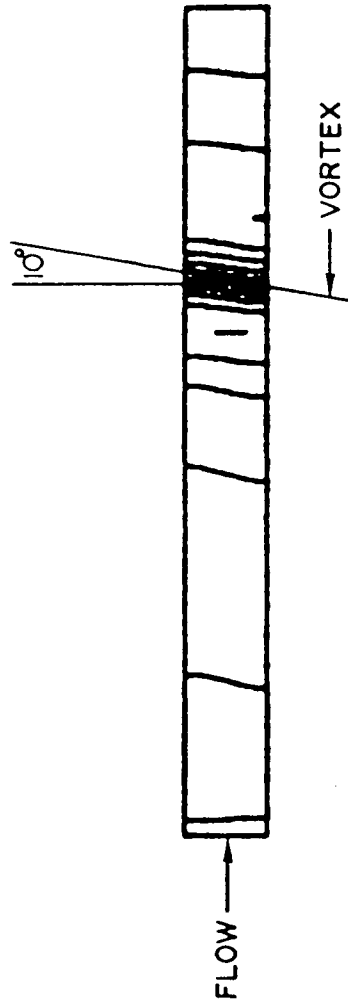
Fig. 14 – Contours of velocity component normal to
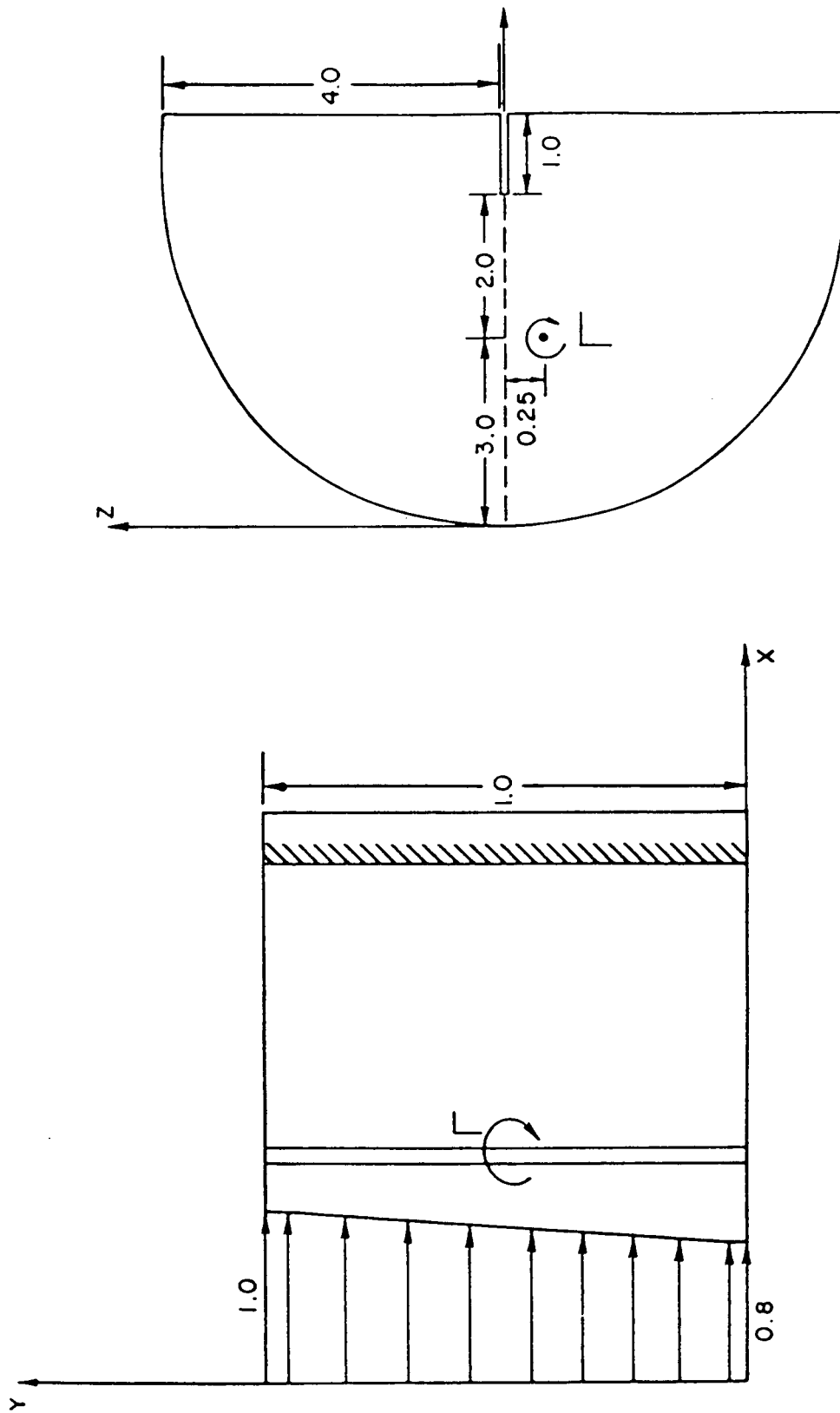the plane through vortex center

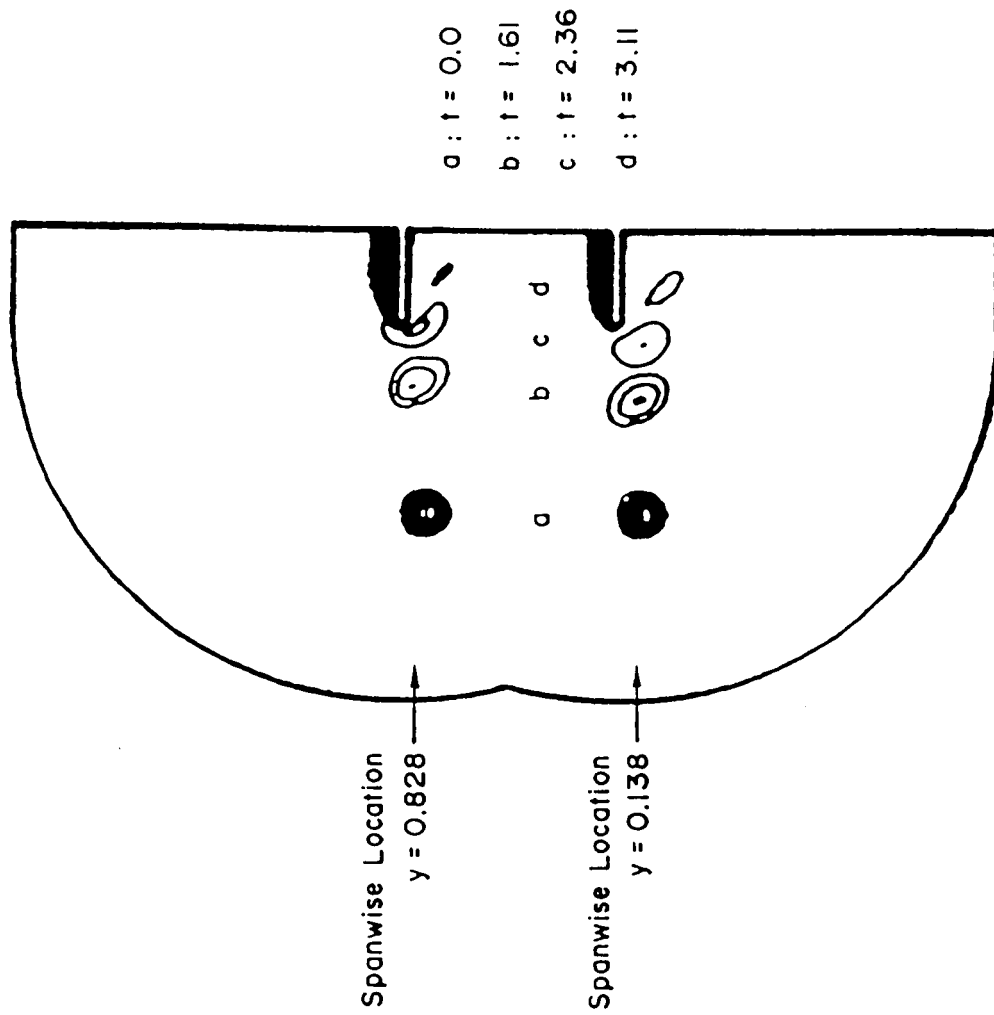Fig. 15 – A schematic of three-dimensional computation of a blade/vortex interaction

Fig. 16 – Vortex movement as a function of time (contours in terms of only positive vorticity of range $0 \leq \Omega \leq 8.0$).
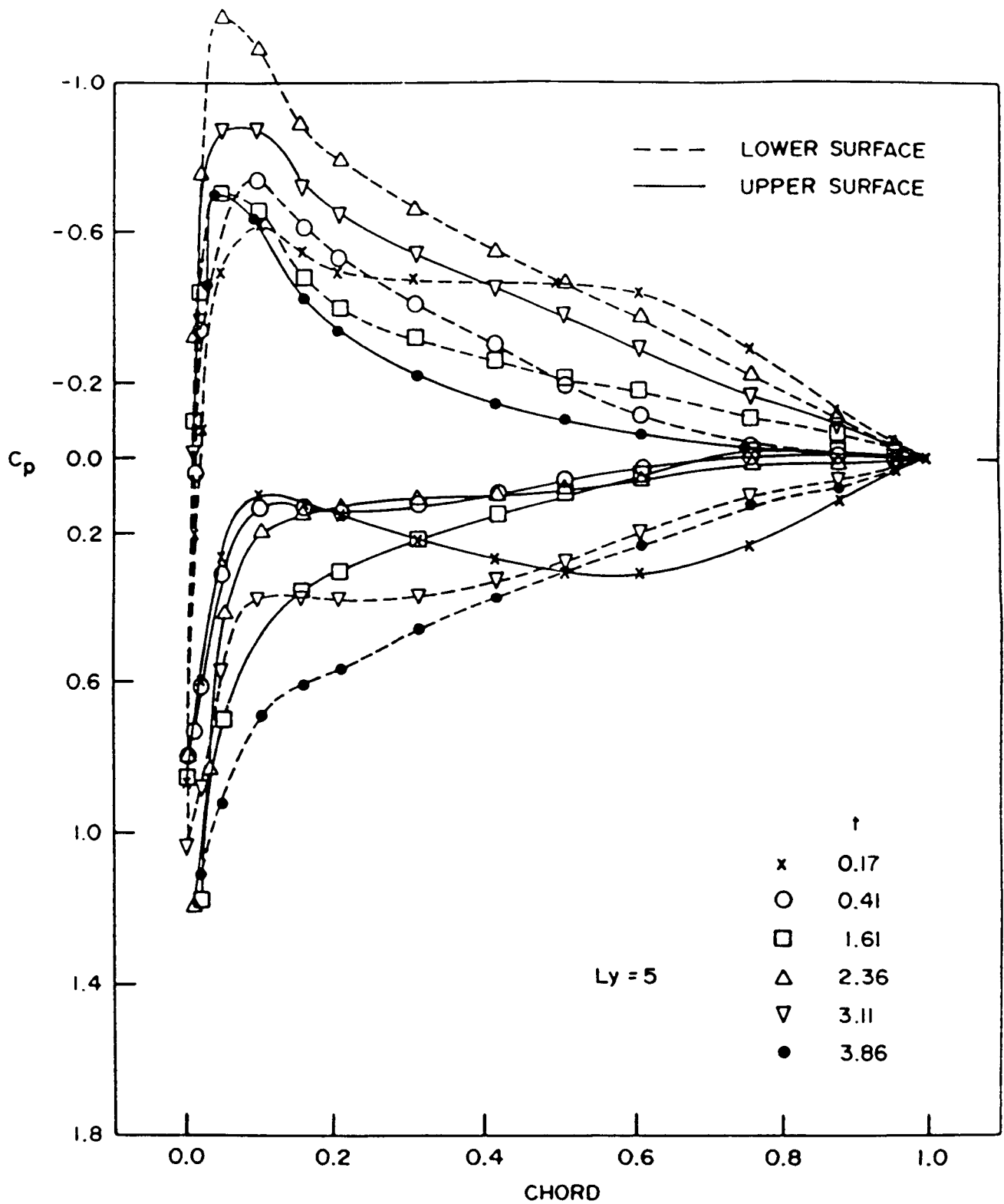
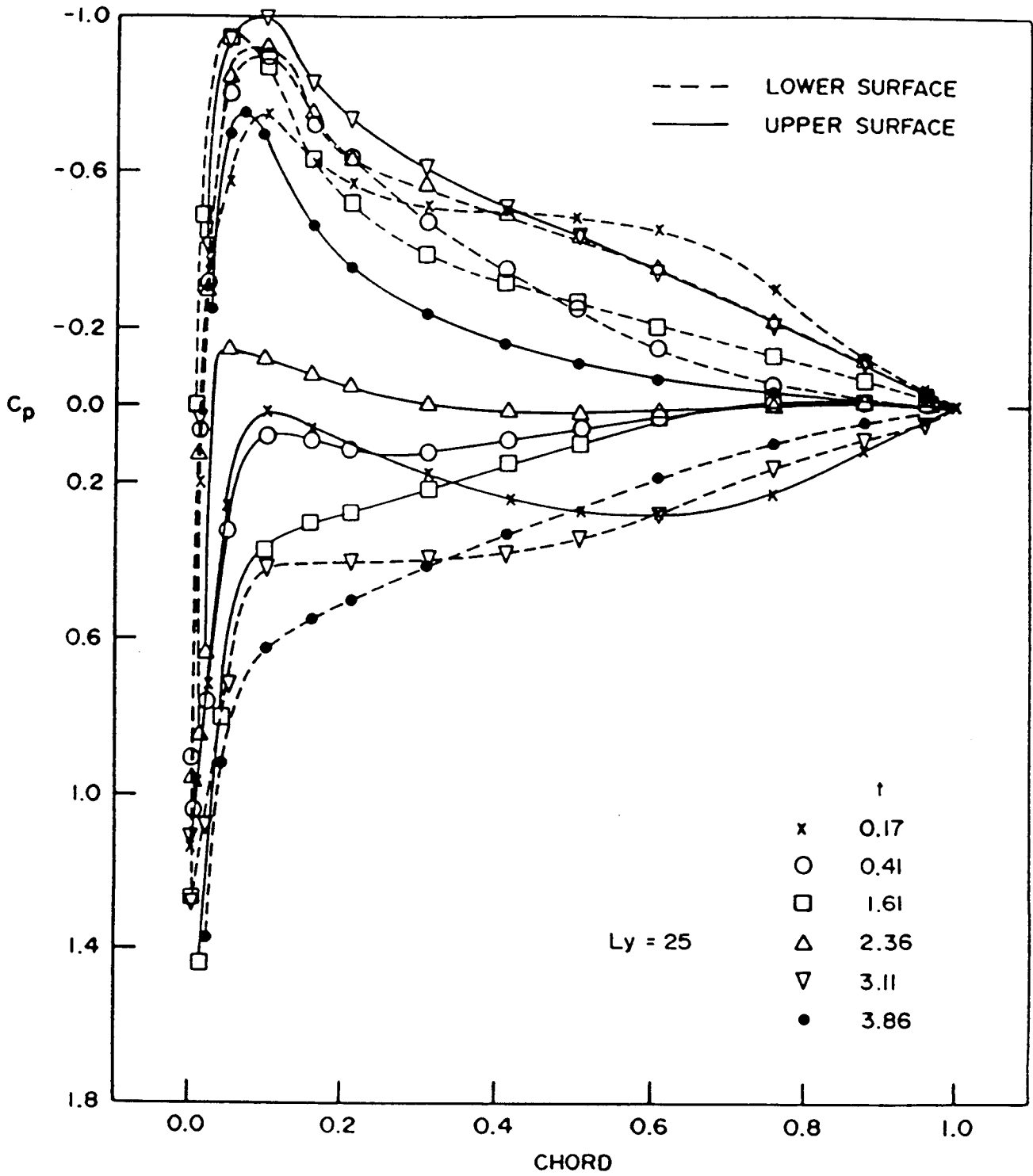Fig. 17 – Unsteady surface pressure distribution
at spanwise location (y = 0.828)

Fig. 18 — Unsteady surface pressure distribution at spanwise location (y = 0.138).

The effects of non-zero intersection angle during the three-dimensional interaction can be seen very clearly; for example, at t = 2.36, represented by the symbol Δ in both Figs. 17 and 18. The vorticity contours at y = 0.828 indicate that the center of the vortex core passed the leading edge. On the other hand, vortex core at y = 0.138 is still located upstream of the leading edge due to the slower convection velocity as expected. The sectional lift force acting in the negative direction at y = 0.138 is larger than that at y = 0.828, as other two-dimensional calculations by both the present authors and other investigators indicated. This clearly demonstrates the capability of the Navier-Stokes calculation procedure for the analysis of three-dimensional blade/vortex interactions.

CONCLUSIONS

The present effort has demonstrated capability of the Navier-Stokes procedure to compute the time-dependent flow field when a vortex filament passes underneath the blade, as in the case of a helicopter. A simple, but effective method of modeling a tip vortex encountering a blade at arbitrary angle was developed and utilized in the computation. Both two-dimensional BVI and three-dimensional vortex/sheared flow interactions were considered. The two-dimensional studies showed the qualitative nature of the interaction previously shown by other investigators in regard to the time dependent behavior of the surface pressure distribution. The three-dimensional simulation required an intersection angle between the vortex and the blade which was non-zero. This was created by immersing the vortex in a spanwise shear flow and a three-dimensional simulation was performed. A qualitative assessment of the results was made and the expected flow features were shown.

REFERENCES

Beam, R.M. and Warming, R.F.: An Implicit Factored Scheme for the Compressible Navier-Stokes Equations. AIAA Journal, Vol. 16, 1978, p. 393.

Briley, W.R. and McDonald, H.: Solution of the Multidimensional Compresible Navier-Stokes Equations by a Generalized Implicit Method, J. Comp. Physics, Vol. 24, pp. 372-297, 1977.

Briley, W.R. and McDonald, H.: On the Structure and Use of Linearized Block Implicit Schemes, J. Comp. Physics, Vol. 34, 1980, pp. 54-73.

Briley, W.R., McDonald, H. and Shamroth, S.J.: A Low Mach Number Euler Formulation and Application to Time Iterative LBI Schemes. AIAA Journal, Vol. 21, 1983.

Caradonna, F.X., Desopper, A. and Tung, C.: Finite-Difference Modeling of Rotor Flows Including Wake Effects, NASA TM-84280, 1982.

Douglas, J. and Gunn, J.E.: A General Formulation of Alternating Direction Methods. Numerische Math., Vol. 6, 1964, pp. 428-453.

George, A.R. and Chang, S.B.: Flow Field and Acoustics of Two-Dimensional Blade-Vortex Interactions, AIAA Paper 84-2309, Oct. 1984.

Hardin, J.C. and Lamkin, S.L.: Aeroacoustic Interaction of a Distributed Vortex with a Lifting Joukowski Airfoil, AIAA Paper 84-2287.

Hsu, T.-M. and Wu, J.C.: Theoretical and Numerical Studies of a Vortex-Airfoil Interaction Problem, AIAA Paper 86-1094.

Johnson, W.: Recent Developments in Rotary-Wing Aerodynamic Theory. AIAA Journal, Vol. 24, August 1986.

Kaykayoglu, R. and Rockwell, D.: Vortices Incident Upon a Leading Edge: Instantaneous Pressure Fields, J.F.M., Vol. 156, pp. 439-461, 1985.

Liu, N.-S., Shamroth, S.J. and McDonald, H.: On Hairpin Vortices as Model of Wall Turbulence Structure, Fifth Symposium on Turbulent Shear Flow, Cornell University, 1985.

McCroskey, W.J.: Special Opportunities in Helicopter Aerodynamics. Recent Advances in Aerodynamics, A. Krothapalli and C.A. Smith (eds.), Springer-Verlag, 1986.

McCroskey, W.J. and Goorjian, P.M.: Interactions of Airfoils with Gusts and Concentrated Vortices in Unsteady Transonic Flow, AIAA Paper 83-1691, June 1983.

McCroskey, W.J. and Srinivasan, G.R.: Transonic Interactions of Unsteady Vortical Flows, Third Symposium on Numerical and Physical Aspects of Aerodynamic Flows, California State University, Long Beach, CA Jan. 21-24, 1983.

Pulliam, T.H. and Steger, J.L.: Implicit Finite Difference Simulations of Three-Dimensional Compressible Flow, AIAA Journal, Vol. 18, 1980, p. 159.

Rai, M.M.: Navier-Soktes Simulations of Blade-Vortex Interaction Using High-Order Accurate Upwind Schemes. AIAA Paper 87-0543, AIAA 25th Aerospace Sciences Meeting, Reno, 1987

Schmitz, F.H. and Yu, Y.H.: Helicopter Impulsive Noise: Theoretical and Experimental Status. Recent Advances in Aeroacoustics, A. Krothapalli and C.A. Smith (eds.), Springer-Verlag, 1986.

Shamroth, S.J., McDonald, H. and Briley, W.R.: Prediction of Cascade Flow Fields Using the Averaged Navier-Stokes Equations, J. Engr. for Gas Turbines and Power, 1984, Vol. 106, p. 383.

Srinivasan, G.R., Chyu, W.J. and Steger, J.L.: Computation of Simple Three-Dimensional Wing Vortex Interaction in Transonic Flow, AIAA Paper 81-1206, AIAA 14th Fluid and Plasma Dynamic Conference, June 1981, Palo Alto, CA.

Srinivasan, G.R., McCroskey, W.J. and Kutler, P.: Numerical Simulation of a Vortex with a Stationary Airfoil in Transonic Flow, AIAA Paper 84-0254, Jan. 1984.

Thomas, P.D. and Lombard, C.K.: Geometric Conservation Law and its Application to Flow Computations on Moving Grids, AIAA Journal, Vol. 17,No. 10, pp. 1030-1037, 1979.

Ting, L.: Studies on the Motion and Decay of a Vortex Filament, Advances in Fluid Mechanics, Ed. E. Krause, pp. 67-105, 1980, Springer-Verlag.

Warming, R.F. and Beam, R.M.: On the Construction and Application of Implicit Factored Schemes for Conservation Laws, Symposium on Computational Fluid Dynamics, New York, April 1977; SIAM-AMS Proceedings, Vol. 11, 1977.

Report Documentation Page

1. Report No. NASA CR-177441	2. Government Accession No.	3. Recipient's Catalog No.

4. Title and Subtitle Calculation of Helicopter Rotor Blade/Vortex Interaction by Navier-Stokes Procedures	5. Report Date April 1987
	6. Performing Organization Code

7. Author(s) Y.-N. Kim, S. J. Shamroth, R. C. Buggeln Scientific Research Associates Glastonbury, CT	8. Performing Organization Report No.
	10. Work Unit No. 324-01-08

9. Performing Organization Name and Address NASA Ames Research Center Moffett Field, CA 94035	11. Contract or Grant No. NAS2-12363
	13. Type of Report and Period Covered Contractor Report Final

12. Sponsoring Agency Name and Address National Aeronautics and Space Administration Washington, D. C. 20546	14. Sponsoring Agency Code

15. Supplementary Notes
   Point of contact: Cahit Kitaplioglu
                       NASA Ames Research Center
                       M/S TR-032
                       Moffett Field, CA 94035
                       (415)694-6679 or FTS 464-6679

16. Abstract

Interactions of a modern rotor blade with concentrated tip vortices from the previous blades can have a significant influence on the airloads and the aeroacoustics of a helicopter. A better understanding of the blade/vortex interaction process and a method of analyzing its flow field would provide valuable help in the design of helicopters. The work discussed herein represents an initial effort in applying a three-dimensional, time-dependent Navier-Stokes simulation to the blade vortex interaction problem. The numerical technique is the Linearized Block Implicit (LBI) technique of Briley and McDonald. In this initial effort, consideration is given to the interaction of a wing of idealized geometry and a vortex whose axis is aligned at an arbitrary angle to the wing. The calculations are made for laminar, subsonic flow and show the time dependent pressure distribution and flow fields resulting from the interaction.

17. Key Words (Suggested by Author(s)) HELICOPTER ROTOR AERODYNAMICS BLADE/VORTEX INTERACTION CFD NAVIER-STOKES AEROACOUSTICS	18. Distribution Statement Unlimited

19. Security Classif. (of this report) Unclassified	20. Security Classif. (of this page) Unclassified	21. No. of pages	22. Price

PREPARATION OF THE REPORT DOCUMENTATION PAGE

The last page of a report facing the third cover is the Report Documentation Page, RDP. Information presented on this page is used in announcing and cataloging reports as well as preparing the cover and title page. Thus it is important that the information be correct. Instructions for filling in each block of the form are as follows:

Block 1. Report No. NASA report series number, if preassigned.

Block 2. Government Accession No. Leave blank.

Block 3. Recipient's Catalog No. Reserved for use by each report recipient.

Block 4. Title and Subtitle. Typed in caps and lower case with dash or period separating subtitle from title.

Block 5. Report Date. Approximate month and year the report will be published.

Block 6. Performing Organization Code. Leave blank.

Block 7. Author(s). Provide full names exactly as they are to appear on the title page. If applicable, the word editor should follow a name.

Block 8. Performing Organization Report No. NASA installation report control number and, if desired, the non-NASA performing organization report control number.

Block 9. Performing Organization Name and Address. Provide affiliation (NASA program office, NASA installation, or contractor name) of authors.

Block 10. Work Unit No. Provide Research and Technology Objectives and Plans (RTOP) number.

Block 11. Contract or Grant No. Provide when applicable.

Block 12. Sponsoring Agency Name and Address. National Aeronautics and Space Administration, Washington, D.C. 20546-0001. If contractor report, add NASA installation or HQ program office.

Block 13. Type of Report and Period Covered. NASA formal report series; for Contractor Report also list type (interim, final) and period covered when applicable.

Block 14. Sponsoring Agency Code. Leave blank.

Block 15. Supplementary Notes. Information not included elsewhere: affiliation of authors if additional space is re-

quired for block 9, notice of work sponsored by another agency, monitor of contract, information about supplements (film, data tapes, etc.), meeting site and date for presented papers, journal to which an article has been submitted, note of a report made from a thesis, appendix by author other than shown in block 7.

Block 16. Abstract. The abstract should be informative rather than descriptive and should state the objectives of the investigation, the methods employed (e.g., simulation, experiment, or remote sensing), the results obtained, and the conclusions reached.

Block 17. Key Words. Identifying words or phrases to be used in cataloging the report.

Block 18. Distribution Statement. Indicate whether report is available to public or not. If not to be controlled, use "Unclassified-Unlimited." If controlled availability is required, list the category approved on the Document Availability Authorization Form (see NHB 2200.2, Form FF427). Also specify subject category (see "Table of Contents" in a current issue of STAR), in which report is to be distributed.

Block 19. Security Classification (of this report). Self-explanatory.

Block 20. Security Classification (of this page). Self-explanatory.

Block 21. No. of Pages. Count front matter pages beginning with iii, text pages including internal blank pages, and the RDP, but not the title page or the back of the title page.

Block 22. Price Code. If block 18 shows "Unclassified-Unlimited," provide the NTIS price code (see "NTIS Price Schedules" in a current issue of STAR) and at the bottom of the form add either "For sale by the National Technical Information Service, Springfield, VA 22161-2171" or "For sale by the Superintendent of Documents, U.S. Government Printing Office, Washington, DC 20402-0001," whichever is appropriate.